JOURNAL OF QUATERNARY SCIENCE (2020) **35**(7) 892–906 ISSN 0267-8179. DOI: 10.1002/jqs.3244

JQS Journal of Quaternary Science QRA Quaternary Research Association

Architecture of tunnel valleys in the southeastern North Sea: new insights from high-resolution seismic imaging

ARNE LOHRBERG,[1]* KLAUS SCHWARZER,[1] DANIEL UNVERRICHT,[1] ANDREAS OMLIN[2] and SEBASTIAN KRASTEL[1]
[1]Christian-Albrechts-Universität zu Kiel, Institute of Geosciences, Kiel, Germany
[2]Geological Survey of Schleswig-Holstein, Flintbek, Germany

Received 27 November 2019; Revised 11 August 2020; Accepted 28 August 2020

ABSTRACT: Tunnel valleys are assumed to form near the margin of ice sheets. Hence, they can be used to reconstruct the dynamics of former ice margins. The detailed formation and infill of tunnel valleys, however, are still not well understood. Here, we present a dense grid of high-resolution 2D multi-channel reflection seismic data from the German sector of the southeastern North Sea imaging tunnel valleys in very great detail. Three tunnel valley systems were traced over distances ranging between 11 and 21 km. All tunnel valleys are completely filled and buried. They differ in incision depth, incision width and number of incisions. The tunnel valleys cut 130–380 m deep into Neogene, Palaeogene and Cretaceous sediments; they show a lower V-shaped and an upper U-shaped morphology. For individual tunnel valleys, the overall incision direction ranges from east–west to northeast–southwest. Two tunnel valleys intersect at an oblique angle without reuse of the thalweg. These valleys incise into a pre-existing glaciotectonic complex consisting of thrust sheets in the northwest of the study area. The analysis of the glaciotectonic complex and the tunnel valleys leads us to assume that we identified several marginal positions of (pre-)Elsterian ice lobes in the southeastern North Sea.

KEYWORDS: glaciogenic unconformity; glaciotectonic complex; ice margin; Quaternary succession; tunnel valleys

Introduction

Major ice sheet advances beyond the polar limits in the northern hemisphere are well documented for the Quaternary (last 2.6 Ma); the last 900,000 years are assumed to be the period with the most prominent ice sheet advances (Ehlers *et al.*, 2018). Understanding the glacial history of continental shelves is key to reconstructing the configuration of former ice sheets. Fortunately, surface and subsurface landforms serve as an archive that can be used to reconstruct past sedimentation and erosion processes. Identifying these landforms and the corresponding mechanisms of formation can support the reconstruction of ice sheet configurations during the Pleistocene (Aber and Ber, 2007; Dowdeswell *et al.*, 2016). Fluctuations in oxygen isotopes found in deep sea cores have been linked to major cold and warm phases of the planet. The rhythmic pattern of gradual cooling and rapid warming of the climate has been defined as Marine Isotope Stages (MIS). The dating of glaciogenic sediments enabled the scientific community to assign the well-known glaciations around the globe to specific MIS (Ehlers and Gibbard, 2004).

Many glacial landforms, e.g. mega-scale glacial lineations, trough-mouth fans, grounding-zone wedges, moraines, drumlins, iceberg ploughmarks, hill-hole pairs, eskers, crag-and-tails, tunnel valleys and glaciotectonic complexes (GTCs) produced by the Elster (MIS 12), Saale (MIS 6 + 8) and Weichsel (MIS 2–6) ice sheets in northern Europe are well documented (Woodland and Woodland, 1970; Ehlers *et al.*, 1984; Ehlers, 1990; Huuse & Lykke-Andersen, 2000; Stewart & Lonergan, 2011; Dowdeswell *et al.*, 2016; Winsemann *et al.*, 2020). A growing body of evidence expands the traditional view of three major glaciations and relates such landforms to more glacial phases and also pre-MIS12 ice sheets in northern Europe (Batchelor *et al.*, 2019; Winsemann *et al.*, 2020). Such landforms have also been documented in North America as a result of the Quaternary glaciations (Wright, 1973; Mullins and Hinchey, 1989; Patterson, 1994; Clayton *et al.*, 1999; Dowdeswell *et al.*, 2016). On land, the surface morphology can be used to identify these landforms; offshore, such landforms are often buried beneath the seafloor. Tunnel valleys and GTCs are the largest and best-preserved subsurface glacial landforms identified in the North Sea.

Tunnel valleys are defined as elongated depressions incised into bedrock or unconsolidated sediment (Ó Cofaigh, 1996; van der Vegt *et al.*, 2012; Kehew *et al.*, 2012). Most studies conclude that tunnel valleys result from subglacial palaeo-drainage channels with high flow rates of meltwater eroding valleys into the sediment and bedrock (Ussing and Selskab, 1903; Moores, 1989; Ghienne and Deynoux, 1998; Lonergan *et al.*, 2006). Still, there is no consensus on whether the erosion mechanism is predominantly based on a 'steady-state' or a 'catastrophic' drainage. The 'steady-state' hypothesis assumes the drainage of pressurised groundwater gradually eroding a subglacial channel, which is broadened by fluvial erosion and direct glacial erosion (Boulton and Hindmarsh, 1987; Kehew *et al.*, 2012; van der Vegt *et al.*, 2012). The 'catastrophic' hypothesis assumes subglacial and supraglacial ponding and accumulation of meltwater and subsequent sudden drainage leading to the incision (Wright, 1973; Lewis *et al.*, 2006).

Interest in tunnel valleys has grown as their potential as hydrocarbon reservoirs and aquifers for meteoric freshwater has become increasingly relevant (Huuse, 2002; van der Vegt *et al.*, 2012). Hence, the detailed study of tunnel valley formation and architecture has multiple benefits: (1) reconstruction of former ice sheet dynamics (Ehlers, 1990; Huuse & Lykke-Andersen, 2000;

*Correspondence: A. Lohrberg, as above.
E-mail: arne.lohrberg@ifg.uni-kiel.de

Stewart & Lonergan, 2011); (2) identification of potential Quaternary freshwater and Ordovician hydrocarbon reservoirs (Sandersen and Jørgensen, 2003; Le Heron *et al.*, 2004; BURVAL Working Group, 2009; Huuse *et al.*, 2012) and improvement of our understanding of subglacial meltwater properties (Greenwood *et al.*, 2016); and (3) improvement of vulnerability concepts for groundwater extraction from tunnel valleys (Sandersen and Jørgensen, 2003; Piotrowski, 2007).

Numerous studies have demonstrated the high abundance of tunnel valleys in the North Sea (Fig. 1a, Praeg, 2003; Kluiving *et al.*, 2003; Lonergan *et al.*, 2006; Kristensen *et al.*, 2007; Lutz *et al.*, 2009; van der Vegt *et al.*, 2012; Stewart *et al.*, 2013; Dove *et al.*, 2017; Prins and Andresen, 2019; Ottesen *et al.*, 2020). Few studies, however, have conducted research in the southeastern German North Sea sector between Helgoland and the Eider Valley (Lutz *et al.*, 2009; Winsemann *et al.*, 2020).

We set out in July 2017 with the expedition AL496 (Fig. 1 b) as part of the project Nordfriesland-Süd to map the shelf architecture and to identify glacial landforms in order to investigate the glacial history of the survey area. We present high-resolution seismic reflection data, which provide an insight into tunnel valley morphology and infill in very high detail. We aim to image and reconstruct the internal structure and spatial development of tunnel valleys. The dense grid of 2D reflection seismic sections (Fig. 1 b) serves as the basis for tunnel valley description, classification and spatial extrapolation. This information is used to identify a former ice sheet margin in the German sector of the southeastern North Sea. Additionally, we aim to contribute to the ongoing debate on the formation mechanism of tunnel valleys.

Methods

We acquired 2D reflection seismic and parametric sediment echo sounder data to image subsurface structures from 0 to 800 ms corresponding to approx. 640 m beneath the seafloor (1600 m/s is used for all time–depth conversions in the absence of a precise velocity model [Cotterill *et al.*, 2017; Coughlan *et al.*, 2018]). A total of 1058 km of 2D high-resolution multi-channel reflection seismic data were acquired in a closely spaced 2D grid covering approximately 800 km^2 (Fig. 1 b). We focus on the analysis of the 2D reflection seismic data because these data show sufficient penetration to image the submerged palaeolandscape.

2D multi-channel reflection seismics acquisition

A Sercel Mini GI gun was used in a harmonic mode with a reduced volume of 0.1 L for both the generator and injector chambers for all seismic lines. The main frequency of the source is approximately 300 Hz. A Geometrics GeoEel solid state digital streamer was used to record the seismic response. Our setup included a 35 m tow cable (30 m in water), a 10 m stretch, and seven active sections, each containing eight channels with a channel spacing of 1.56 m. This resulted in 56 active channels and an active streamer length of 87.5 m. The broad frequency spectrum of the source (70–600 Hz) allowed us to image deep sediments as well as to correlate the shallow strata with the simultaneously acquired sediment echo sounder data. The vertical resolution is in the metre range; maximum resolution of about 1 m is achieved in the upper tens of metres below the seafloor. Resolution slightly decreases with increasing penetration due to absorption of high frequencies.

Seismic data processing

This study followed standard reflection seismic processing routines in Schlumberger's Vista Seismic Processing software: (1) Ormsby frequency filtering (55/110 and 600/1200 filter flanks); (2) CMP binning; (3) FK-filtering; (4) normal moveout (NMO) correction using a velocity model based on interactive picking of best-fit velocities; (5) despiking; (6) CMP-stacking; and (7) finite-differences time-migrating these data with a velocity model inferred from an interactive velocity analysis. A shot point distance of 9 m or less allowed the common midpoint (CMP) bin spacing to be set equal to the channel spacing of 1.56 m, resulting in a CMP fold of 6 to 10.

Further special processing involved the removal of multiple reflections, which interfered with primary reflectors due to the very shallow water depth (less than 25 m). Removal of both seafloor and internal reflector multiples was accomplished using a fine-tuned predictive deconvolution with an adapted lag time based on picks of the seafloor and the first multiple.

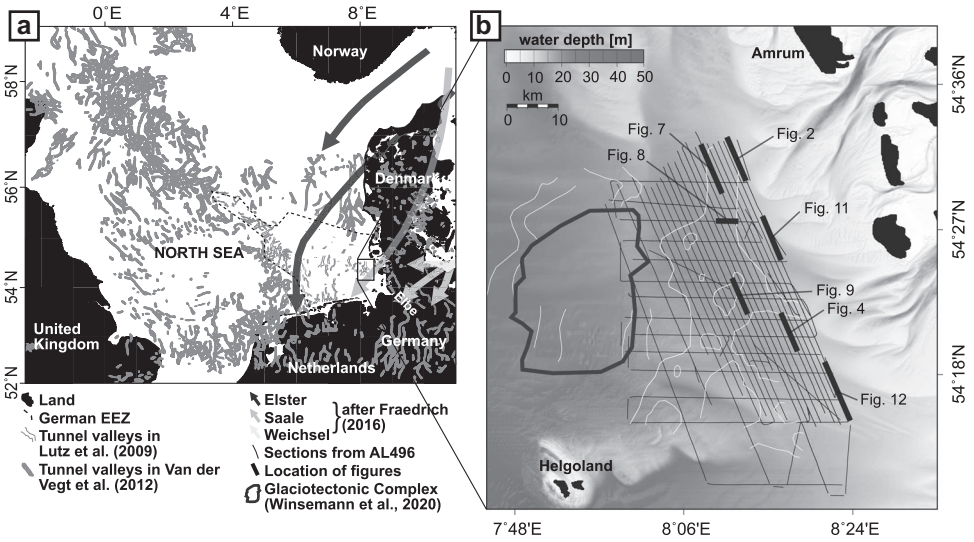

Figure 1. Overview maps showing the location of the study area and the survey grid. (a) Compilation of tunnel valleys mapped in the German sector of the North Sea (Lutz *et al.*, 2009) and for the remaining North Sea (van der Vegt *et al.*, 2012). The study area is marked with a black rectangle. (b) Grid of seismic sections available from expedition AL496 and bathymetry of the survey area provided by the Federal Maritime and Hydrographic Agency of Germany (GeoSeaPortal, 2019). Tunnel valleys from Lutz *et al.* (2009) are indicated as white lines.

This approach yielded very good results owing to the flat seafloor throughout the study area.

Seismic data interpretation

The fully processed seismic sections were loaded in the IHS Markit Kingdom Software 2017 for interpretation. Kingdom was used to trace horizons and the morphology of subsurface landforms. The horizons were exported for interpolation and plotting with the Generic Mapping Tools open-source software.

Results

The stratigraphic units and subsurface landforms shown in this section were identified based on differences in acoustic properties on the seismic sections. To focus on the description of the tunnel valleys, we refrain from providing a detailed seismostratigraphical analysis of the seismic sections. Instead, we use a more general approach delineating the seven main seismic units (SU) up to 800 ms penetration that have been correlated to the seismic stratigraphy framework of the Federal Agency of Geosciences and Resources of Germany (BGR), which is based on the results of Thöle *et al.*, 2014 and Kockel, 2002. Table 1 outlines the correlation of the SU defined here with the stratigraphic framework of the BGR, which includes well control from many deep wells in the German sector of the North Sea.

Stratigraphy of the working area

The seismic sections in the north of the study area reveal the complete sedimentary sequence of the upper Cretaceous to the Quaternary (Fig. 2). Seven SU were identified. Fig. 3 outlines the depth to the major boundaries during late Cretaceous to late Miocene identified as continuous reflectors in the subsurface. These sediments are overlain by Plio-Pleistocene sediments, which build the foundation for the Holocene drape (Thöle *et al.*, 2014).

SU1 is the deepest seismic unit characterised by slightly undulating, continuous reflectors of very low amplitude (Fig. 2). Its top is defined by a continuous reflector of significantly higher amplitude than the otherwise very low amplitude reflectors of the thick sedimentary package. This reflector is found at 730 ms two-way-travel-time (TWT; ~580 m) (Figs 2 and 3a). Deposits of SU1 represent Cretaceous sediments (Table 1, Thöle *et al.*, 2014).

SU2 is the thickest seismic unit. It is characterised by a transition in seismic facies in the upper third of the unit (at 525 ms, 420 m on the seismic section shown in Fig. 2). Beneath this transition, these data image a thick package of continuous reflectors of very low amplitudes, whereas the reflections show increased amplitudes above the transition. SU2 includes several reflector packages characterised by high amplitudes at their base and low amplitudes at their top (Fig. 2, 525 ms to 475 ms, 420 to 380 m and 440 ms to 400 s, 350 to 320 m). Its shallowest section is characterised by well-stratified low amplitude reflectors. The deposits of SU2 represent Palaeogene sediments (Table 1, Thöle *et al.*, 2014).

SU3 consists of reflectors characterised by an alternating high to medium amplitude pattern from 400 ms (320 m) upwards. The high to medium amplitudes dominate up to 240 ms (190 m), where amplitudes decrease to medium to low. A narrow high amplitude reflector characterises its top, which represents the mid-Miocene unconformity. The mid-Miocene unconformity is truncated by the Quaternary succession (Fig. 3, Lutz *et al.*, 2009) in the central and southern part of the study area and is thus absent from parts of our study area. A high amplitude continuous reflector marks the base of SU3 (Fig. 2), which has been correlated to represent lower to late Miocene sediments (Table 1, Thöle *et al.*, 2014).

SU4 is only found in the northern part of the study area. The abrupt change in seismic facies to very low amplitude reflectors topped by three sharp high amplitude reflectors characterises this unit (Fig. 2). The pattern of alternating high amplitude to low amplitude reflectors, as seen in the underlying units, is absent here (Fig. 2). This clearly delineates SU4 from SU3. The deposits of SU4 most likely represent Pliocene to early Pleistocene sediments because they are constrained by Miocene sediments at their base and the Quaternary succession at their top (Table 1). Due to the lack of data, an unambiguous correlation with Pliocene sediments is not feasible.

SU5 is characterised by alternating strong and weak reflectors in its lower part, which transitions to chaotic strong reflectors in the upper part (Fig. 2). Tracing of reflectors is feasible only in the lower part. The onset of deformation in the lower parts of SU5 delineates this unit from SU4 and links SU5 to the Quaternary succession (Fig. 2, Table 1). SU5 is thus comprised of mainly Pleistocene sediments that are truncated at its top throughout the study area.

SU6 demarcates the erosional flanks and the fill of tunnel valleys (Fig. 2). These tunnel valley complexes truncate SU1–SU5. SU6 often shows a lower V-shaped unit and an upper U-shaped unit, imaged by a change in flank steepness and a change in seismic facies (Fig. 2). Chaotic low to medium amplitude reflections characterise the lower V-shaped subunit, whereas medium to high amplitude reflectors of good

Table 1. Stratigraphic basis for the interpretation of the subsurface strata. Main reflectors delineating the seismic units (SU) have been correlated with the stratigraphic framework of the Federal Agency of Geosciences and Resources of Germany (BGR), which is based on the results of Kockel (2002) and Thöle *et al.* (2014)

Epoch	Stratigraphic unit		BGR base reflector	Duration (Ma)	This study
Quaternary	Pleistocene, Holocene		q	1.8	SU5 + SU6 + SU7
Neogene	Pliocene?		tpl	3.5	SU4
	Miocene	MMU	tmi	18.5	SU3
Palaeogene	Oligocene		tol	9.9	SU2
	Eocene		teo	21.1	
	Seelandian/Thanetian		tpao	6.1	
	Danien, Montian		td	4	
Cretaceous	Maastrichtian		krma	6.3	SU1
	Campanian		krca	12.2	
	Santonian		krsa	2.3	

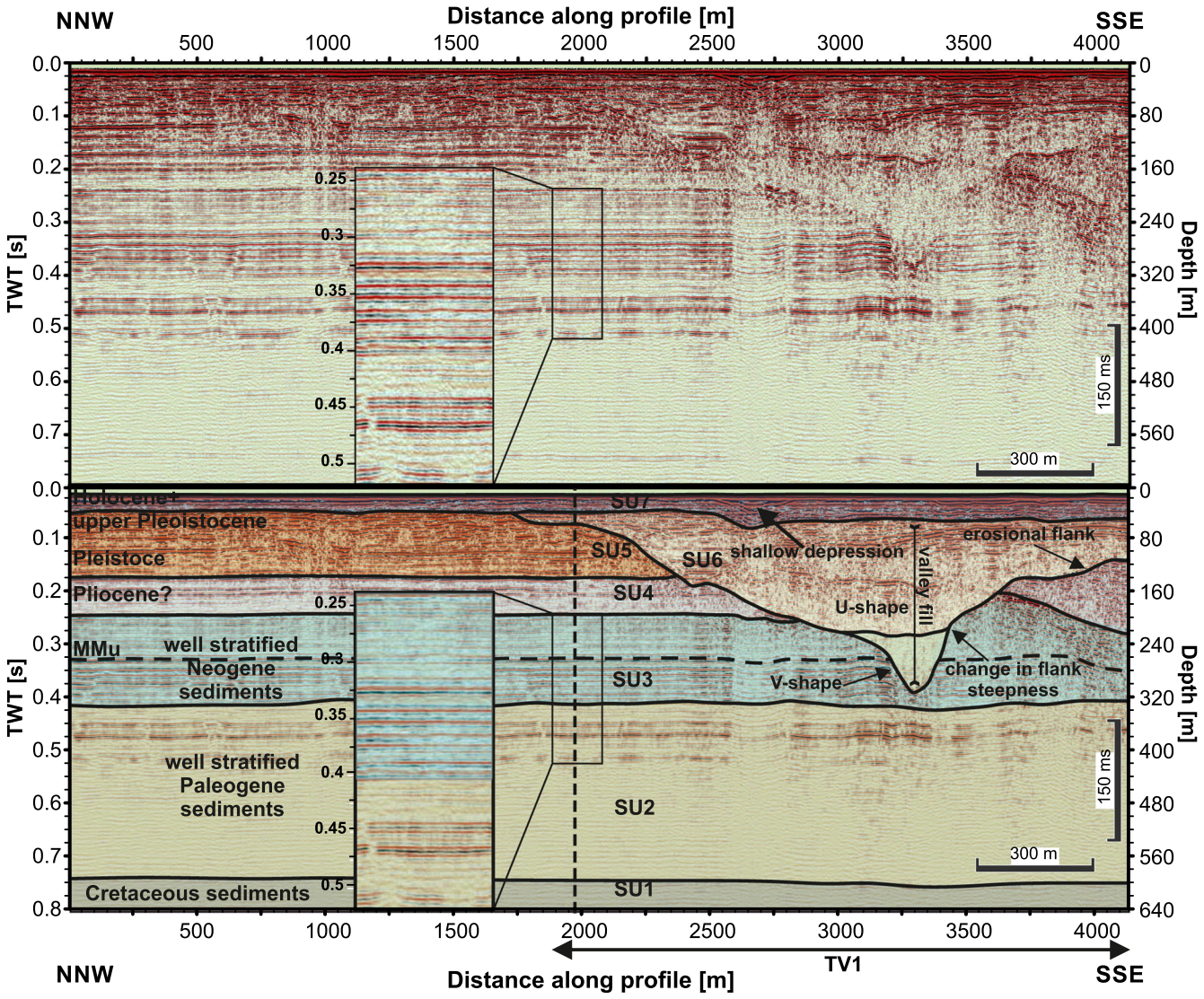

Figure 2. Stratigraphy of the study area. All seven seismic units (SU) were traced throughout the study area, where they have not been eroded by the Quaternary succession. The close-up details the amplitude patterns of SU2b and SU3. Dashed line is the reference line for the description of the units. [Color figure can be viewed at wileyonlinelibrary.com]

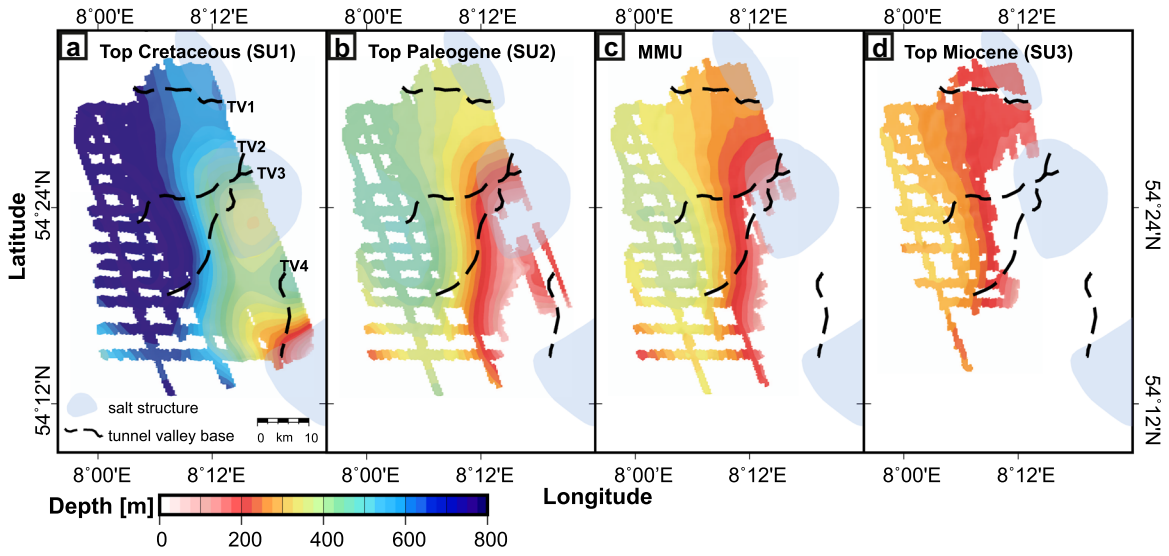

Figure 3. Depths to top of stratigraphic units and the outline of salt structures. Each subplot displays the regional morphology of the top of the seismic units. SU4–6 are not laterally continuous and are thus excluded. SU7 represents the flat seafloor. All subplots clearly show an influence of the underlying salt structures 'Karla' (centre) and 'Rochelsteert' (south), which led to the deformation of sediments in the study area. [Color figure can be viewed at wileyonlinelibrary.com]

continuity characterise the upper U-shaped subunit (Fig. 2). Reflectors of the upper U-shaped subunit are sometimes inclined and differ in thickness between individual tunnel valleys. SU6 includes up to four prominent reflectors, which represent subsequent incisions into the tunnel valleys (see 'Tunnel valley morphology, internal structure and spatial extent', below).

SU7 is the shallowest seismic unit and its top represents the seafloor (Fig. 2). Its surface is flat throughout the study area. SU7 truncates SU5 and SU6 (Fig. 2). This truncation is represented by an erosional surface that represents the base of SU7. Shallow elongate depressions resembling small channels (up to 300 m width) are often found in SU7 (e.g. Fig. 2 at 25 ms TWT, 20 m, and 2550 to 2800 m along profile). The top sediments of SU7 represent Holocene deposits, whereas the lower sediments of SU7 represent late Pleistocene deposits resting unconformably on SU5 and SU6.

Glaciogenic unconformity

A glaciogenic unconformity has been described before for wide areas of the southern North Sea (Moreau *et al.*, 2012) as well as for the southern Baltic Sea (Al Hseinat and Hübscher, 2014). It formed during the Quaternary succession likely by glacial erosion and is identified based on reflectors lying unconformably on Neogene or older strata. The glaciogenic unconformity has thus been recognised as the onset of the Quaternary, on top of which ice sheets have deposited sediments during the Pleistocene.

The glaciogenic unconformity in the study area is represented by prominent glacial erosional surfaces and the tunnel valley systems, which truncate the lower units SU1–SU4. On top of this unconformity, SU5 and SU6 have been deposited and thus represent the Quaternary succession (Sejrup *et al.*, 1991). The high spatial heterogeneity and often ambiguous seismic representation of the glacial erosional surfaces complicates tracing them reliably over longer distances (Fig. 4). The connection of tunnel valley flanks and glacial erosional surfaces can be used to link both features to the same time of formation.

Tunnel valley morphology, internal structure and spatial extent

We mapped three overdeepened buried glacial valley systems consisting of five large tunnel valleys and several smaller valleys (Fig. 5). We focus on characterising the five largest and fully imaged valleys that we traced unambiguously on neighbouring lines. From tracing the landforms over parallel seismic sections, we reconstructed the lateral and vertical extent of the tunnel valleys and a GTC (Fig. 5). Individual plots for TV1–TV3's base reveals an undulating thalweg (Fig. 6). For the sake of clarity, we named the individual main valleys TV#. The fill of the main valleys is denoted by TV#f# and their internal erosional surfaces are denoted as TV#e#.

Although partly surveyed on its edge, the northernmost valley is the broadest and deepest valley with a width of up to 4.5 km and incision depth up to 480 ms (~380 m), (Figs 5 and 7). It is termed tunnel valley 1 (TV1) from hereon. TV1 is characterised by erosional truncations of the surrounding sediments (TV1e1 incised into SU2–SU5) and a subsequent deposition of sediments inside the valley (TV1f1–4 in SU6, Fig. 7). The southern flank of TV1e1 is imaged as a strong reflector and is sharper and steeper (up to 19°) than the northern flank (note that Fig. 7 is roughly eight times vertically exaggerated). The northern flank of TV1e1 is broader, less pronounced (missing a clear seismic reflector) and shallower (approximately 6°). Undisturbed layering of the surrounding strata to the north of the valley (approximately 60 ms to maximum imaging depth at approximately 800 ms) highlights TV1's sharp incision flanks (Fig. 7). Stratification inside this valley is generally not very pronounced and absent in its deeper part; chaotic reflections with low amplitudes and low continuity dominate the deeper part (TV1f1) and preclude the tracing of reflectors. Overall, the valley fill (TV1f1–4) is divided by erosional unconformities marking the different incisions (TV1e2–4), which partly result in sharp seismic reflectors. Two major incisions of 350 ms (280 m) by TV1e1 and 260 ms (210 m) by TV1e2 and a third incision of smaller magnitude up to 100 ms (80 m) by TV1e3 can be identified in TV1 (Fig. 7). The latest incision cuts older incisions at the top (TV1e4). These erosional surfaces delineate several stages in the cut-and-fill structures, which indicate that TV1e1 predates TV1e2, which predates TV1e3, which predates TV1e4. Weak layering is seen in TV1f4,

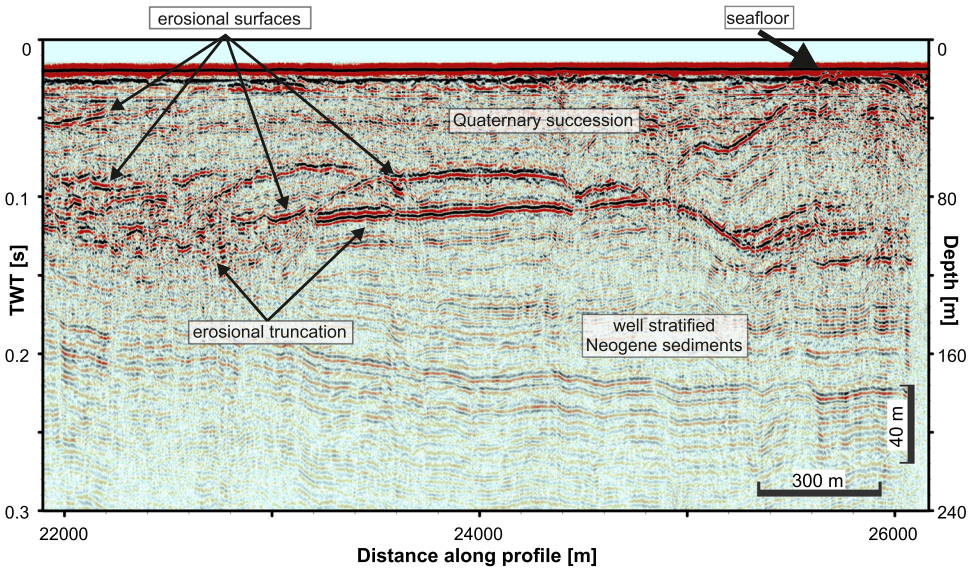

Figure 4. Example of erosional unconformities defining the glaciogenic unconformity in the centre of the study area imaged as strong reflectors. Layering is strong in the strata beneath and nearly absent from the strata above the glaciogenic unconformity. [Color figure can be viewed at wileyonlinelibrary.com]

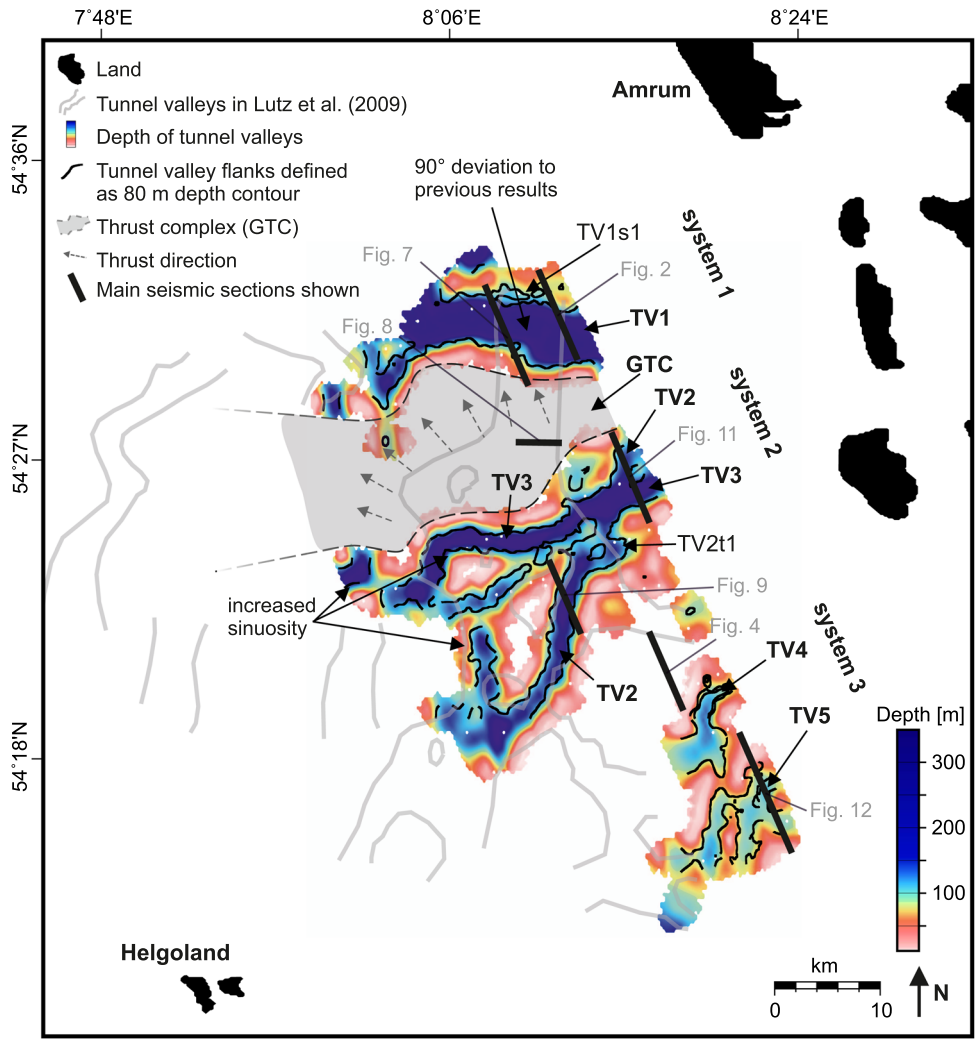

Figure 5. Distribution of tunnel valleys in the study area. Colours give incision depths; black contour lines mark the tunnel valley flanks defined at 80 m depth; grey dashed line outlines extent of a glaciotectonic complex; bold grey lines indicate tunnel valleys interpreted by Lutz *et al.* (2009). [Color figure can be viewed at wileyonlinelibrary.com]

which corresponds to the upper approximately 30 m of the valley fill. A side valley (TV1s) is located north of its northern flank at a distance of approximately 250 m (Figs 5 and 7), whose lower part connects to TV1e1. A strong reflector at the top of TV1s connects to TV1e3, thus linking the lower fill to TV1f1 and the fill above the reflector to TV1f3.

A GTC has been identified in the northwestern part of the survey area (Fig. 5). Several sheets with a thickness of up to 100 ms (80 m) have been thrust towards the north to northwest (Fig. 7). The GTC initiates below an updipping prominent glacial erosional surface between TV1 and TV2 (Fig. 8) and the thrust sheets dominate the shallow substratum up to 200 ms (160 m) depth in the northwest of the survey area. TV1 cuts the northernmost limit of the GTC (Fig. 7).

Tunnel valley 2 (TV2) cuts approximately 210 ms (170 m) deep and can be traced for about 20 km from northeast to southwest (Figs 5, 9, 11). The seismic section in Fig. 9 images two prominent reflectors in the strata next to the base of TV2 comprised of north–northwest dipping nearly undisturbed sediments (SU3), clearly incised by TV2e1 and TV2e2 (at 18300 to 18700 m along profile). The average width of TV2 is approximately 1.5 km (Fig. 5). The infill of TV2 is well stratified on most seismic sections, often showing a larger upper U-shaped unit (TV2f2, SU6b) and a comparably small lower V-shaped unit with less internal stratification (TV2f1, SU6a; Figs 9 and 10). The change in seismic facies correlates with the change in flank steepness (Fig. 10). Tracing TV2 from east to west on the perpendicular seismic sections reveals that it originates in the east from well-layered sediments deposited on top of the broad U-shaped base (TV2f2, Fig. 11 at 10400–12500 m along profile). The eastern U-shaped base (TV2e2) shows small depressions in its western rim (Fig. 11 at 12 150 m and 190 ms, 150 m). The upper valley fill stratification (TV2f2) dips slightly towards the south–southeast. Westward of the profile shown in Fig. 11, the tunnel valley fill develops into a pattern characterised by the absence of layering in the lower V-shaped unit, whereas its upper U-shaped part remains stratified (Fig. S2 plots c–f). In the central part of the study area, TV2 has a tributary valley (TV2t1), which joins TV2 about 1.9 km further southwest (Fig. 5).

Tunnel valley 3 (TV3) runs approximately west–southwest to east–northeast (Fig. 5) and intersects TV2. Tracing the erosional base of both tunnel valleys (TV2e1 and TV3e1) from the easternmost sections towards the west (Figs S2 and S3), it is clear that the valleys initiated as individual valleys in the east. After a few kilometres, they intersect and then separate again (Figs 1 and 11). TV3 clearly does not reuse TV2's thalweg, which can be seen at their intersection (Fig. 11) and parallel seismic sections (Figs S2 and S3). Instead, TV3e1 cut TV2 and progressed towards the west. TV3's width is about 1.5 km, similar to TV2 (Fig. 11). TV3 can be traced for about 18 km. It is incised deeper than TV2 with a mean incision depth of 280 ms (~220 m) and a maximum incision depth of 300 ms (~240 m) into the deposits of SU2 and SU3 (Fig. 11). On the

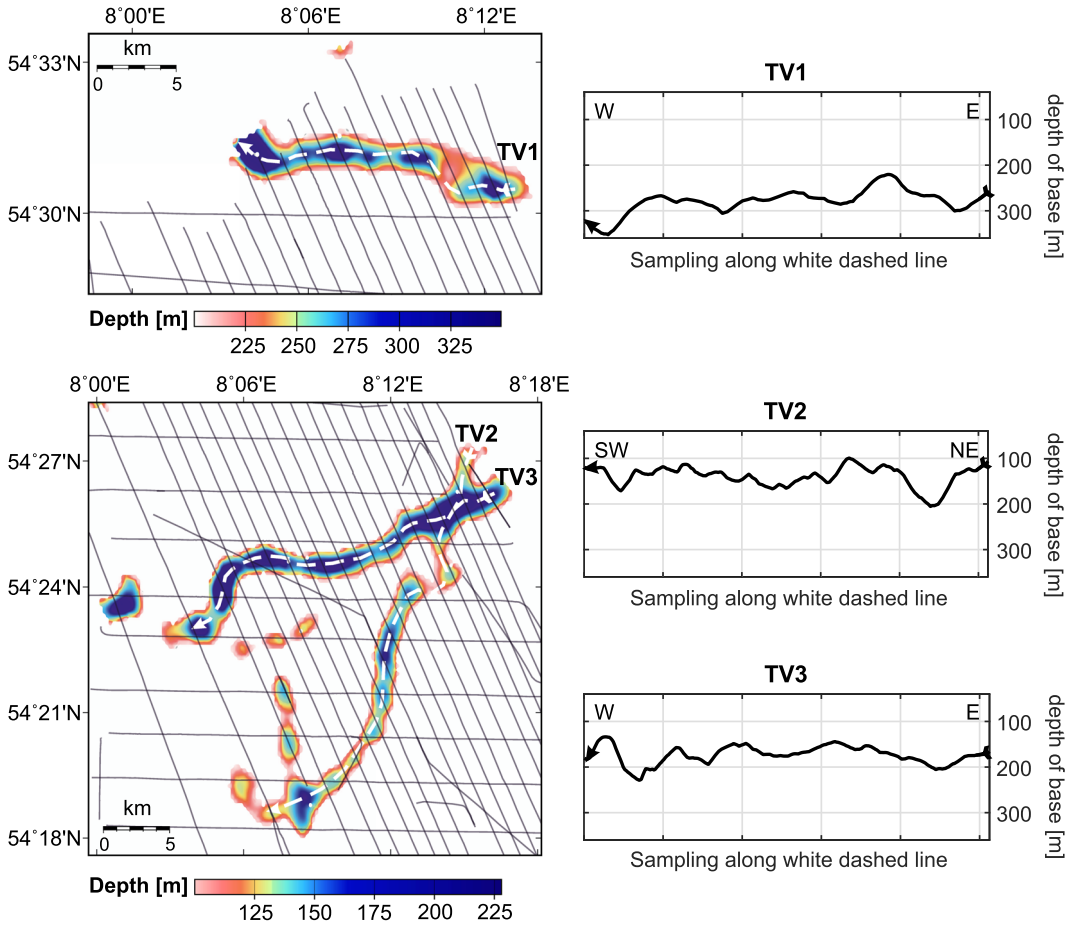

Figure 6. Morphology and long profiles of the lower chaotic V-shape subunit (SU6a) of TV1–TV3. Vertical undulations along the thalweg are clearly visible for all tunnel valleys, both in the morphology grid (left) and the long profiles (right). [Color figure can be viewed at wileyonlinelibrary.com]

western seismic sections, TV3's lower unit (TV3f1) consists of a chaotic facies but becomes increasingly stratified above (TV3f2) (Fig. S3). Disturbed reflectors in the strata beneath the tunnel valley spatially coincide with the change in flank steepness.

The central valleys TV2 and TV3 differ from TV1 in their internal structure and size. They are narrower and incisions into the pre-existing sediments are shallower (Fig. 5). TV2 and TV3 can be separated in plan view based on their mean incision depths alone, which are more or less constant along their thalwegs (Fig. 5).

The southern valley complex consists of two main valleys, TV4 and TV5 (Fig. 12 at 8700–11300 m and 11300–13200 m along profile), and smaller side valleys (Fig. 12 at 8600–9200 m along profile). These tunnel valley complexes show significantly shallower incision depths of up to 160 ms (approximately 130 m). The flanks connect to a shallow glacial erosional unconformity towards the north (Fig. 12 at 6500–8000 m along profile). Their infill (TV4f1 and TV5f1) is mostly stratified and usually has only a minor lower unit without stratification. TV4e1 and TV5e1 are asymmetric with steeper northern flanks and less inclined southern flanks (Fig. 12). In contrast to the northern valleys (TV1–TV3), TV4 and TV5 are underlain by both inclined Palaeogene (SU2 and SU3) and Cretaceous (SU1) sediments and thus incised into different strata (Fig. 12). The dip of the southern flank of TV4 even matches the dip of the underlying strata (Fig. 12). Fig. 5 illustrates that tracing TV4 and TV5 is ambiguous compared with the northern valleys, despite the dense line spacing. However, the overall incision direction is roughly towards the southwest.

Glaciotectonic structures in the subsurface

Large thrust sheets dominate the shallow part of the subsurface below the Holocene and upper Pleistocene sediments in the northwest (Figs 5, 7, 8, S1) and minor thrust sheets are found just south of TV2 (Figs 9 and S2). The thrust sheets display variable thicknesses between approx. 50 and 100 m and lengths varying between 300 and 800 m depending on their location (shorter in the southeast, longer in the northwest). All thrust sheets are based by undisturbed strata (e.g. Fig. 7) acting as a décollement. The northern extent of thrust sheets is limited by the broad incision of TV1.

Discussion

Distribution of tunnel valleys

In their deepest part, all tunnel valleys observed in this study incise into well-stratified Neogene and late Palaeogene sediments, which were likely deposited within the Eridanos delta sequence (Overeem *et al.*, 2001; Thöle *et al.*, 2014). Two underlying salt structures, probably reactivated during the Alpine Orogeny (Ziegler, 1990), led to the deformation of Palaeogene and Neogene units SU1–SU4 (Fig. 3): salt pillow 'Karla' updomed the subsurface in the centre and salt pillow 'Rochelsteert' updomed the subsurface in the southeastern part of the study area (Lokhorst, 1998). This uplift resulted in glacial erosional truncation of SU2–SU4 during the Quaternary by massive ice sheets and subsequent deposition of Quaternary sediments. Here, tunnel valleys incised into SU2b and SU3 at the flanks of the salt pillow 'Karla' (Figs 9 and 11).

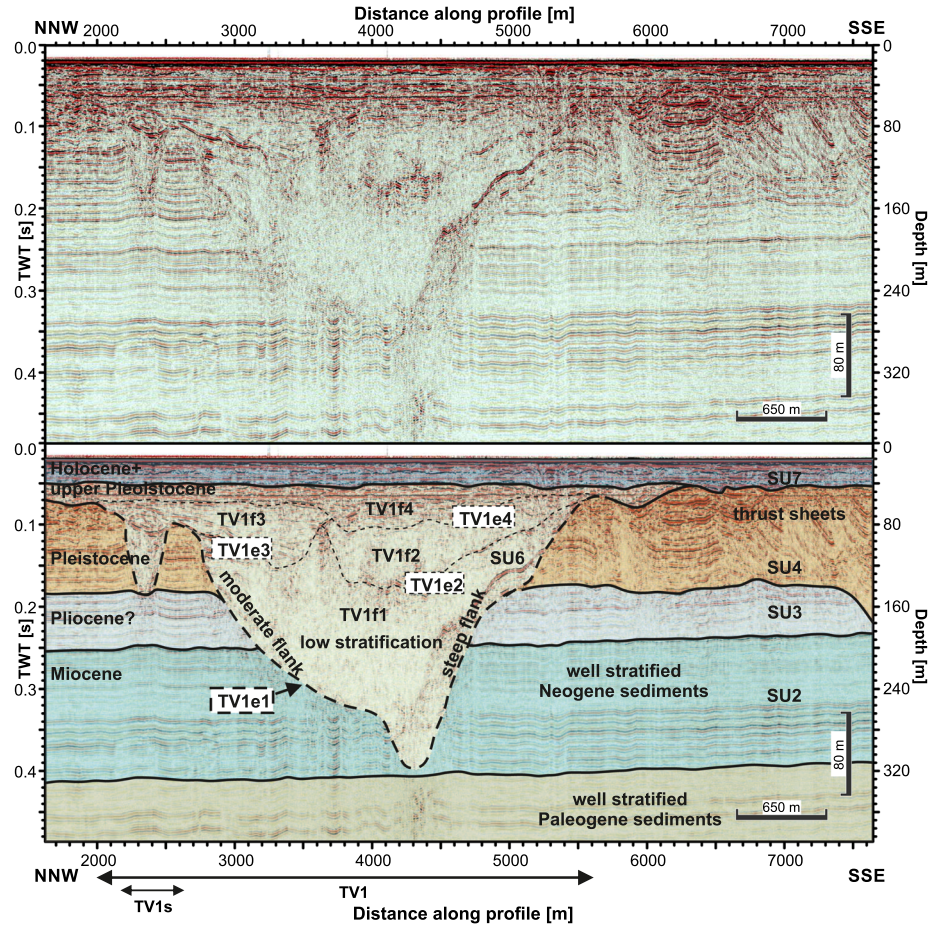

Figure 7 Northernmost tunnel valley (TV1) built from multiple subsequent incisions (TVe1–TVe4). [Color figure can be viewed at wileyonlinelibrary.com]

The subsurface in the southeast shows steeper updoming of sediments (Fig. 3). Tunnel valleys were incised into SU1, SU2 and SU3 in this area (Fig. 12). We consider that the different strata led to asymmetric valley flanks in the southern valley complex (Fig. 11 b), indicating that the difference in underlying strata has influenced the morphology and likely the incision direction of the buried valleys.

However, we are unable to unambiguously validate that the valleys follow a subsurface morphological trend or an associated geological phenomenon, e.g. salt diapirs, as suggested by other authors for other tunnel valleys (Hinsch, 1979; Ehlers and Linke, 1989; Kristensen *et al.*, 2007). Limited by the spatial coverage of our data set, we find that the lateral spacing of the tunnel valleys is more or less constant

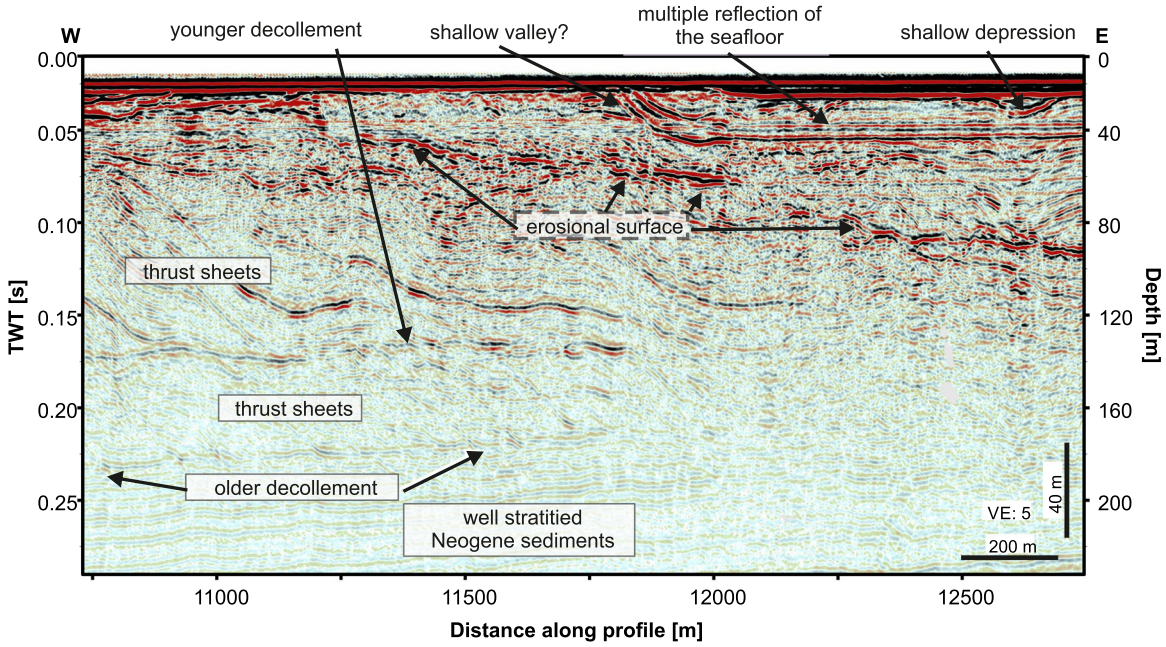

Figure 8. Seismic section showing the updipping erosional unconformity of the central study area and thrust sheets pointing towards the northwest. [Color figure can be viewed at wileyonlinelibrary.com]

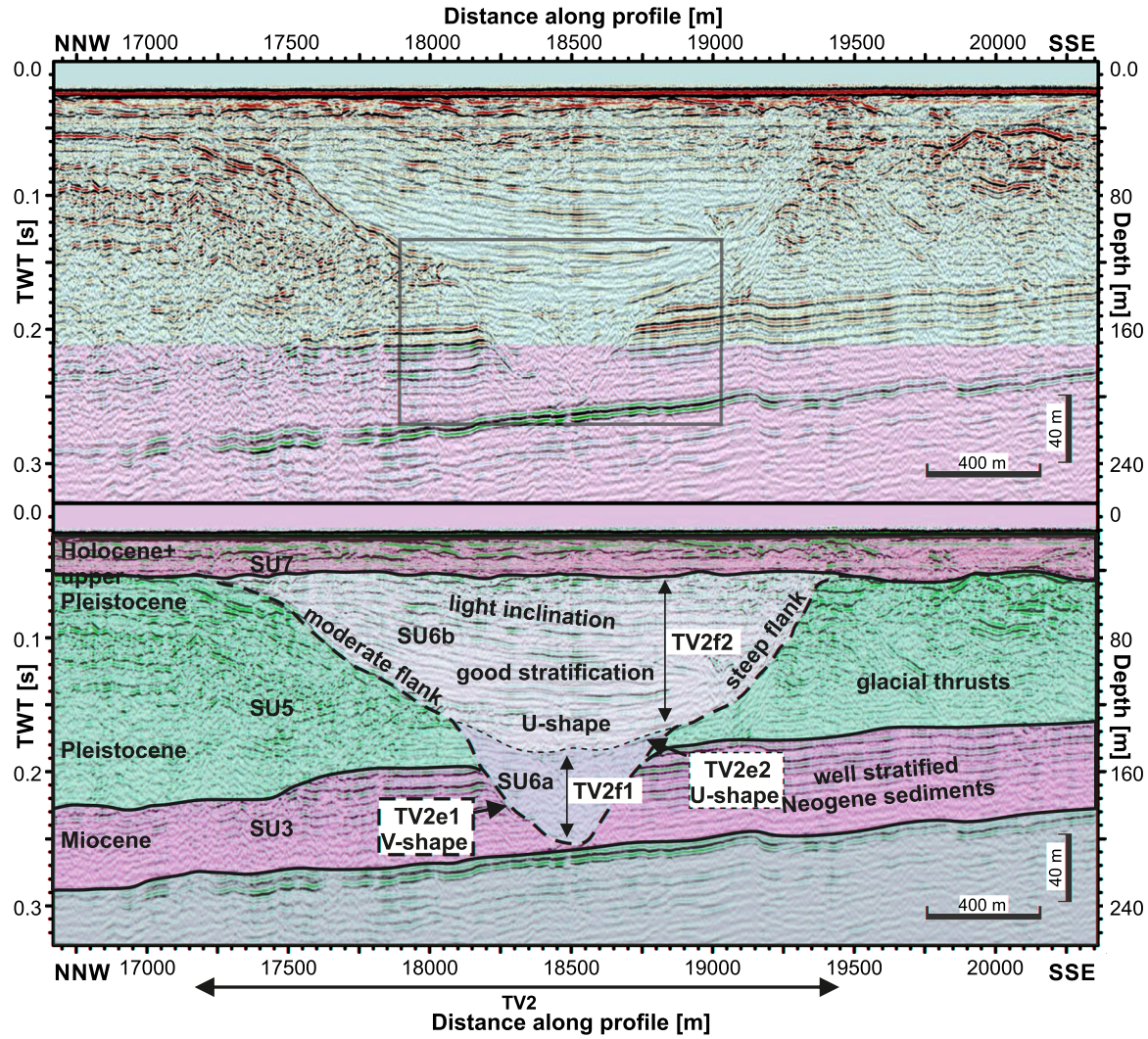

Figure 9. Seismic section crossing a central tunnel valley (TV2) and imaging the structure perpendicular to its incision direction. Internal erosional unconformities are missing, suggesting a single incision for its formation. [Color figure can be viewed at wileyonlinelibrary.com]

and roughly coincides with salt structures in the subsurface. Accordingly, the morphology of the tunnel valleys may be primarily controlled by the lithological variations of the substratum as proposed for other areas of the North Sea (Praeg, 1996), but we can neither validate nor rule out substratum controls on the broader drainage pattern.

Internal structure and morphology of tunnel valleys

The different number of subsequent incisions inside TV1–TV3 likely indicates separate phases of cut and fill, a complex ice margin or a combination of both. TV1's incision phases are clearly delineated by individual erosional surfaces that indicate cut-and-fill structures. A deep initial incision (TV1e1) into the Miocene

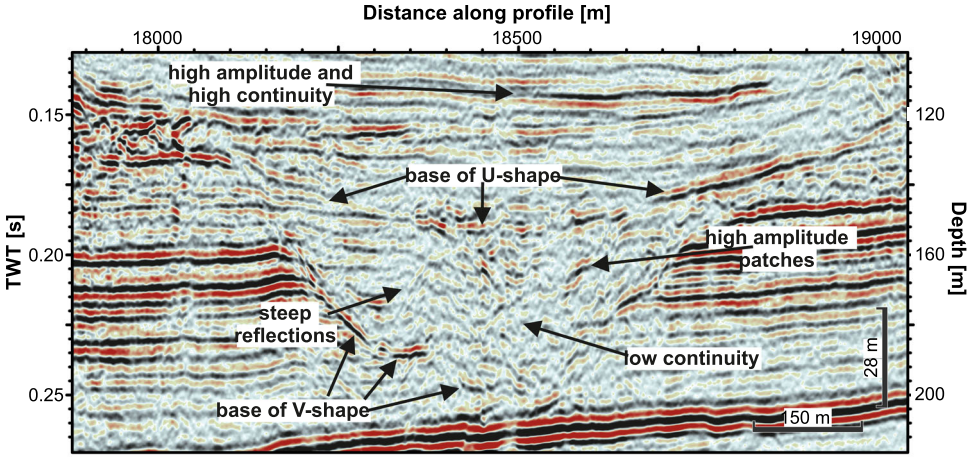

Figure 10. Close-up of the lower V-shaped subunit (SU6a) of TV2. The separation of the tunnel valley fill (TV2f1 + f2) into a lower chaotic subunit (SU6a) and an upper well-stratified subunit (SU6b) is clearly imaged. [Color figure can be viewed at wileyonlinelibrary.com]

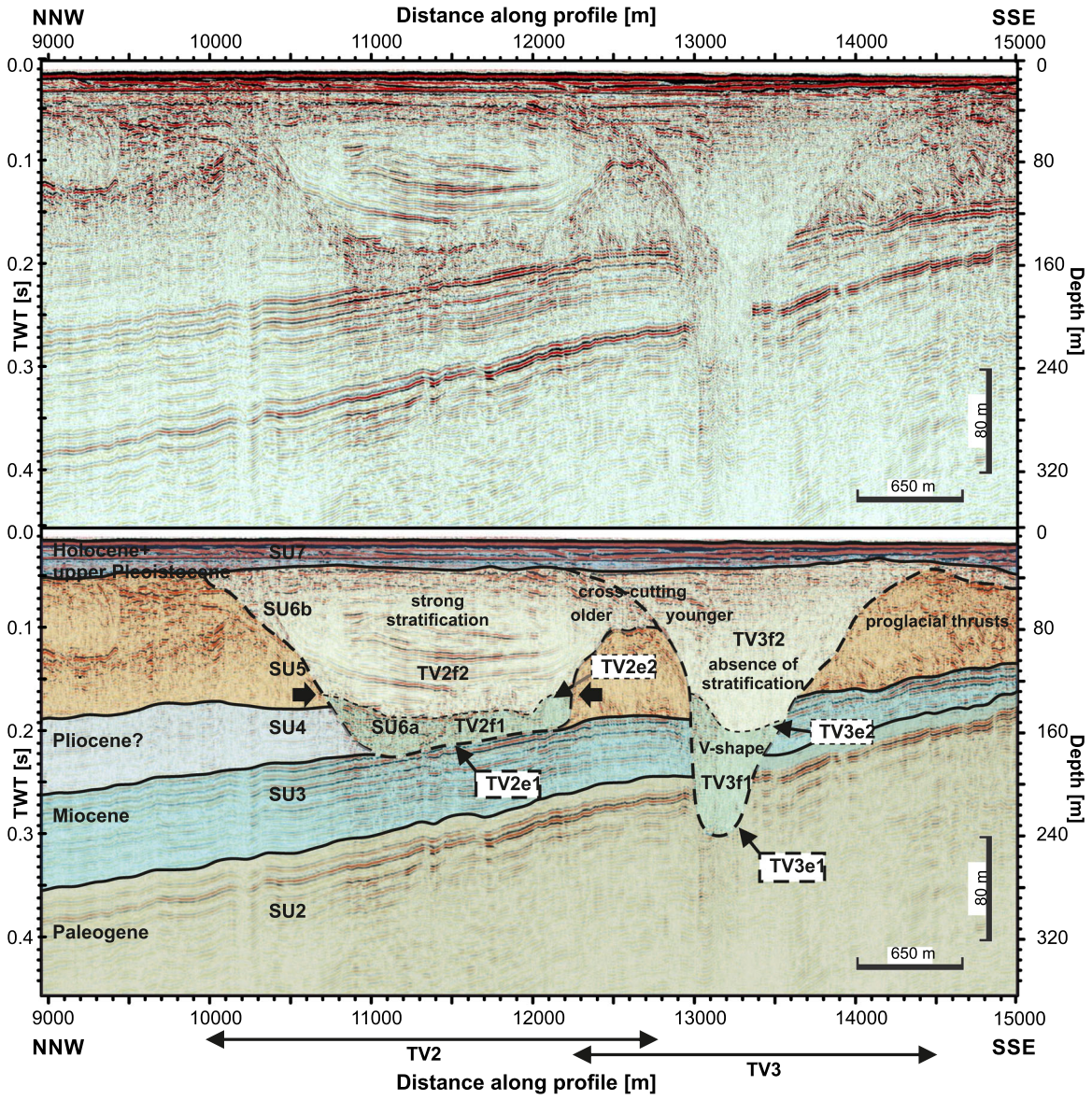

Figure 11. Tunnel valleys of the central study area (TV2 and TV3). TV3 cuts into the fill of TV2, indicating a later formation during a subsequent ice advance. [Color figure can be viewed at wileyonlinelibrary.com]

sediments (SU3) was followed by minor incisions close to either flank (TV1e2–4). The latest incision (TV1e4) widened the tunnel valley complex to its present lateral extent of approximately 4.5 km (Fig. 7). A similar late widening of tunnel valleys has been described for other tunnel valleys in northwest Europe (Piotrowski, 1994; Jørgensen and Sandersen, 2006). Overall dimensions are consistent with other tunnel valleys, which typically range from less than 100 m up to 4–5 km (Woodland and Woodland, 1970; Le Heron *et al.*, 2004; Jørgensen and Sandersen, 2006; Kristensen *et al.*, 2007; Kehew *et al.*, 2012; van der Vegt *et al.*, 2012; Stewart *et al.*, 2013; Livingstone and Clark, 2016). Common depth-to-width ratios have been postulated to be 1:10 (Ghienne and Deynoux, 1998; Gibling, 2006), which is the same order of magnitude as the tunnel valleys investigated here; namely, ratios between 1:10 and 1:20. Flank angles reported in this article of 6 to 19° fall well within the range reported by Kristensen *et al.* (2007) for other Pleistocene tunnel valleys in the North Sea. As neither the beginning nor the end of the tunnel valleys are located in the study area, we are unable to provide slopes for these locations to compare with values given in the literature (e.g. Kristensen *et al.*, 2008; Moreau *et al.*, 2012). However, we do observe morphological undulations along the thalweg (Fig. 6), which has been described as characteristic feature for many tunnel valleys (Huuse & Lykke-Andersen, 2000; Kluiving *et al.*, 2003; Kristensen *et al.*, 2007; Stewart *et al.*, 2013). TV2 and TV3 additionally display a pronounced V-shape in their lower parts, which is usually interpreted as inner gorges (Huuse and Lykke-Andersen, 2000; Kluiving *et al.*, 2003; Kristensen *et al.*, 2007; Stewart *et al.*, 2013; Jansen *et al.*, 2014).

The southern tunnel valley complexes (TV4 and TV5) show the shallowest incision depths. In addition, TV4 and TV5's internal structure does not show an inclination of reflectors and the stratification of the infill (TV4f1 and TV5f1) is well preserved on most seismic sections. Investigation of the southern end of the study area is limited by strong acoustic blanking due to shallow gas, which precludes tracing TV4 and TV5 for more than a few kilometres. The extensive acoustic blanking in our data renders finding the true extent of the southern tunnel valley complex impossible from these data.

Tunnel valley orientation

The incision direction of the tunnel valleys is roughly east–west to northeast–southwest but there are clear differences in the

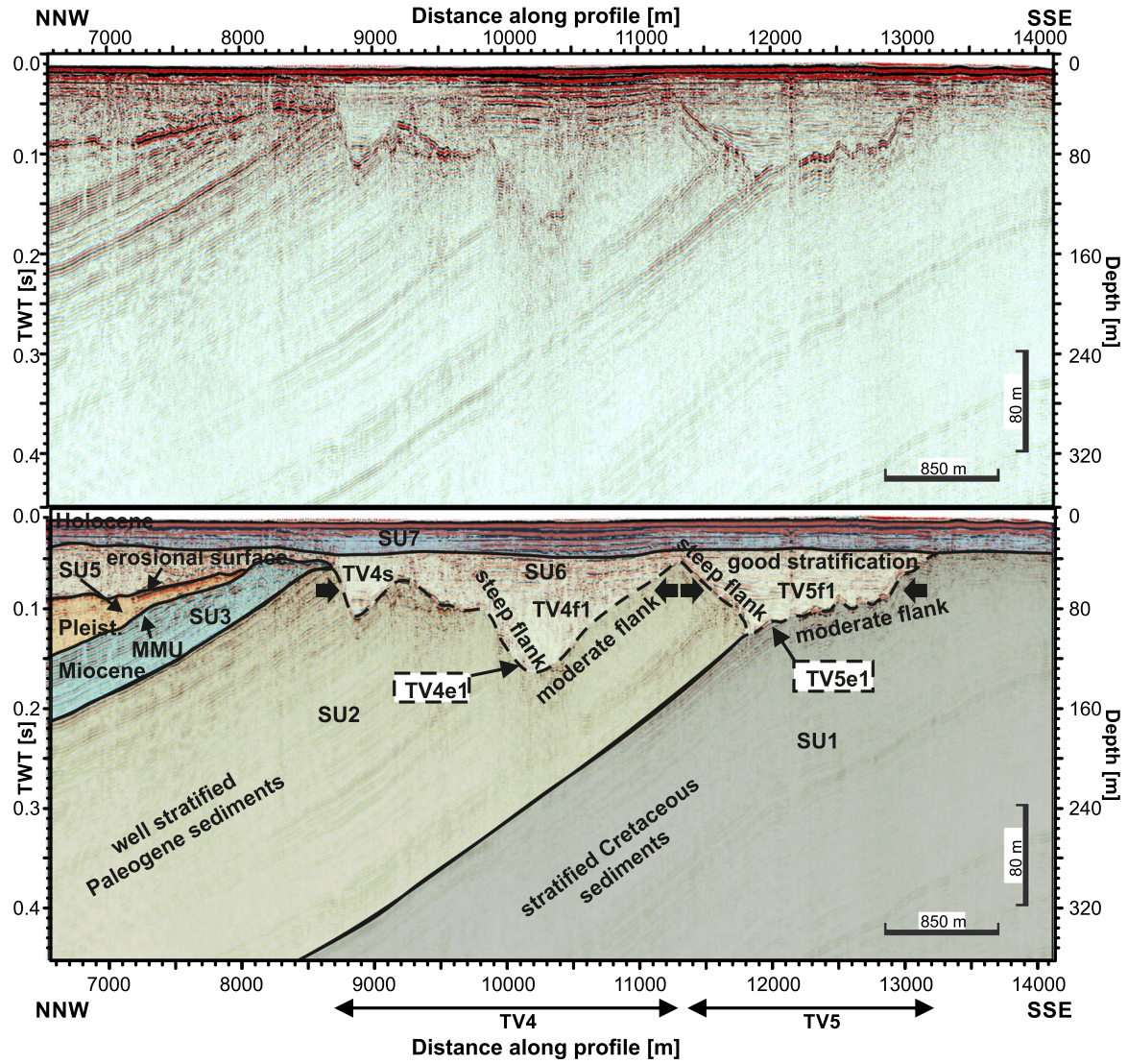

Figure 12. Seismic section imaging TV4 and TV5 in the southeast of the study area. Both show significantly smaller incision depths and smaller width compared with TV1–TV3; subsequent incisions are missing. These tunnel valleys incised into different substrata (SU1 and SU2), which led to different incision depths and asymmetric valley flanks. [Color figure can be viewed at wileyonlinelibrary.com]

incision direction of individual tunnel valleys. For example, incision directions of the crossing valleys TV2 and TV3 clearly differ. The incision direction of TV3 is not influenced by the earlier incision of TV2 (Fig. 5). This lack of reuse of TV2's thalweg indicates that TV2 was already completely filled with sediment during TV3's formation. Consequently, both tunnel valleys document independent incisions (TV2e1 and TV3e1) and a time of sedimentation in between. TV3's average incision depth is significantly deeper than TV2's and the incision is oriented more westward (Fig. 5), representing a change both in magnitude and direction of incision. These differences possibly reflect a change in the ice margin's orientation during the formation of TV3 compared with the formation of TV2. Without precise age control, we are unable to attribute the individual incisions to specific ice advances but we consider it likely that individual incisions were formed during separate ice advances (Winsemann *et al.*, 2020).

Fig. 12 illustrates how different sediments offer different resistance against incision. The difference in resistance results in steep northern flanks and gentle southern flanks, whose dip compares to the dip of the substrate (Ehlers and Linke, 1989; Jørgensen and Sandersen, 2006; Stackebrandt, 2009). The laterally variable substratum in the south influences the incision direction and depth, which is reflected in the complex incision pattern and dip of the flanks of the southern valley complexes TV4 and TV5 (Fig. 5). In contrast, TV1–TV3 incised into mainly Neogene strata with little lateral heterogeneity and overall reduced erosion resistance, which led to higher incision depths, wider valleys and better traceability (Fig. 5) assuming similar magnitudes of drainage and duration.

Comparison with Lutz et al. (2009)

The spatial interpolation of tunnel valleys based on our dense seismic grid led to a 3D model for TV1–TV5, which we used to define valley flanks (Fig. 5). Lutz *et al.* (2009) presented the most recent compilation of the distribution of tunnel valleys in the German sector of the North Sea based on a number of surveys. Fig. 5 provides a comparison with the compilation of Lutz *et al.* (2009). We find that former interpretations of incision directions interpreted before deviate significantly from our results; in parts, incision directions differ by up to 90°, which has implications for the configuration of the former ice sheet margin covering the study area. Furthermore, the width of tunnel valleys differs significantly from earlier studies (Lutz *et al.*, 2009), and tributary tunnel valleys are now visible. Our data reveal greater sinuosity in the west, whereas sinuosity is low or absent in the east (Fig. 5). The comparison also reveals

that a GTC has been previously classified as tunnel valleys (see grey-shaded area in Fig. 5). Here, Lutz *et al.* (2009) postulated a broad tunnel valley, whereas our data clearly show glaciotectonic disturbance of the strata (Figs 7 and 8). Only our new densely spaced data set allowed us to define the true distribution and directions of the tunnel valleys. The mapping of Lutz *et al.* (2009) was based on a broad line spacing and assumed mainly southward ice advances (Figs 1 and 5). This comparison shows that a very close line spacing or 3D seismic data sets are vital to examine the spatial characteristics of tunnel valleys in detail.

Tunnel valley formation

The glaciogenic unconformity terminates towards the west of the study area represented by an upward dipping strong reflector, which spatially coincides with the onset of glaciotectonic thrusting (Fig. 8). The geomorphological characteristics of this unconformity as well as the spatial correlation with glaciotectonic thrusting suggests that this unconformity represents the onset of ice-marginal thrusting, thus reflecting a temporary termination zone of a previous glaciation. To the west, no pre-Holocene glacial erosional unconformities are identified.

Towards the east, multiple glacial erosional unconformities between late Miocene and Holocene strata indicate several phases of glacial erosion. These possibly reflect periods of sea level low stands during glaciations. Based on the assumption that the Elsterian glaciation was the first one to cover vast areas of the North Sea (Ehlers *et al.*, 2011; Winsemann *et al.*, 2020), we suggest that abrasion by an extensive ice lobe during this glaciation led to the deepest glacial erosional unconformity, which connects to TV1–TV3 flanks (Fig. 4). Thus, the deep tunnel valleys incised into Miocene strata and truncating the glacial erosional unconformity likely formed during an Elsterian ice advance.

The separation into V- and U-shapes of the tunnel valley base is unambiguous for TV1–TV3. This morphology and the undulating thalwegs (Fig. 6) would be unexpected to result from fluvial erosion. From the subsurface data alone, it is difficult to identify whether a pre-glacial depression existed that was occupied by an ice stream, and whether subsequent subglacial drainage led to the meltwater erosional surfaces. Any morphological markers of this depression would be eroded by the subsequent incision of tunnel valleys. However, taking into account the undulating thalwegs, steep-sided V-shape inner gorges and overdeep meltwater erosion into significantly older undisturbed strata, we consider it unlikely that the tunnel valleys initially formed in a fluvial regime (Huuse and Lykke-Andersen, 2000; Jansen *et al.*, 2014). Based on the morphological evidence, we therefore opt for a subglacial formation during high-pressure drainage conditions.

TV2 does not show indications of multiple incisions. Consequently, we assume that TV2 may include the complete and undisturbed sedimentation cycle of a filled and buried tunnel valley, assuming that no subsequent drainage event has completely removed a previous infill. The clear separation of a lower V-shaped (inner gorge) and an upper U-shaped unit with the absence of an erosional unconformity (Fig. 11) suggests a single ice advance for its formation.

The southern shallow and more complex tunnel valley systems (TV4 and TV5) are separated from their deeper counterparts (TV1–TV3) by at least one glacial erosional unconformity throughout the study area. This separation suggests that an ice sheet retreat and subsequent ice sheet advance separate their formation (Moores, 1989; Praeg and Long, 1997; Kristensen *et al.*, 2007; Sandersen *et al.*, 2009; Stewart and Lonergan, 2011; Moreau *et al.*, 2012). If we consider the partial lack of internal erosional stages in TV2 and TV3 but assume an Elsterian origin (Lutz *et al.*, 2009), then the shallow glacial erosional unconformities and TV4 and TV5 may have formed during a later glaciation–deglaciation cycle. Previous studies have shown that the Saalian glaciation probably reached the study area (Lambeck *et al.*, 2006), but the Weichselian ice sheets did not (Ehlers, 1990). Therefore, we suggest that the shallow glacial erosional unconformities and connecting valleys (TV4 and TV5) have likely formed during a post-Elsterian glaciation (Winsemann *et al.*, 2020).

Time control for the formation of individual tunnel valleys can only be achieved by direct sampling and dating, but such data are not available. The relative timing of incision does not exclude multiple incisions during a single glaciation. Assuming the formation of all tunnel valleys during a single glaciation–deglaciation cycle would imply that the Saalian glaciation did not produce a prominent glacial erosional unconformity. However, we consider it unlikely that the Saalian ice sheet reached the area without producing a glacial erosional unconformity.

Orientation of former ice margins

The distribution and direction of tunnel valleys provide indications on the configuration of ice sheet margins. Woldstedt (1922) and Huuse & Lykke-Andersen (2000) have established that tunnel valleys usually form within ice sheet margins and that their orientation is usually parallel to ice flow (see van der Vegt *et al.* (2012) and references therein). Following this assumption, the incision directions of tunnel valleys TV1–TV5 indicate ice sheet advances oriented from north to south and northeast to southwest. However, these derived directions conflict with the north–northwest thrust direction of the GTC between TV1 and TV2, which suggests either a change in the orientation of the ice margin between the formation of the GTC and the tunnel valleys, or that the tunnel valleys did not flow perpendicular to the ice sheet margin.

Assuming the formation of tunnel valleys parallel to ice flow during a single stagnating ice advance, the distribution of tunnel valleys indicates an arcuate ice margin (Fig. 13), in analogy to the findings of Benediktsson *et al.* (2015). In this scenario, the GTC formed at the northern to western margin of the ice lobe. The thrusting of sheets towards the northwest indicates that glaciotectonic stress acted along an arcuate ice margin resulting in a change of thrust direction from north to west (Fig. 5). The subsequent multi-phase formation of TV1 may be attributed to drainage of meltwater beneath dynamic ice sheet margins (Fig. 13).

This scenario supports the assumption of an arcuate ice lobe advancing towards the west or southwest. However, it is likely that the GTC and the tunnel valleys formed during a number of ice advances, which matches well both the incision direction of the valleys and the thrust directions of the GTC (Fig. 13). Without dating, we are unable to assign an exact age to the GTC. However, based on the incision of valleys, it is clear that the GTC formed before the tunnel valleys. Assuming the bigger and deeper tunnel valleys (TV1–TV3) formed during the Elsterian glaciation (Lutz *et al.*, 2009; Lang *et al.*, 2012), we suggest an early Elsterian or pre-Elsterian age for the GTC in accordance with Winsemann *et al.* (2020). The morphological features thus likely document a number of ice advances into the southeastern North Sea with different orientations (Fig. 13).

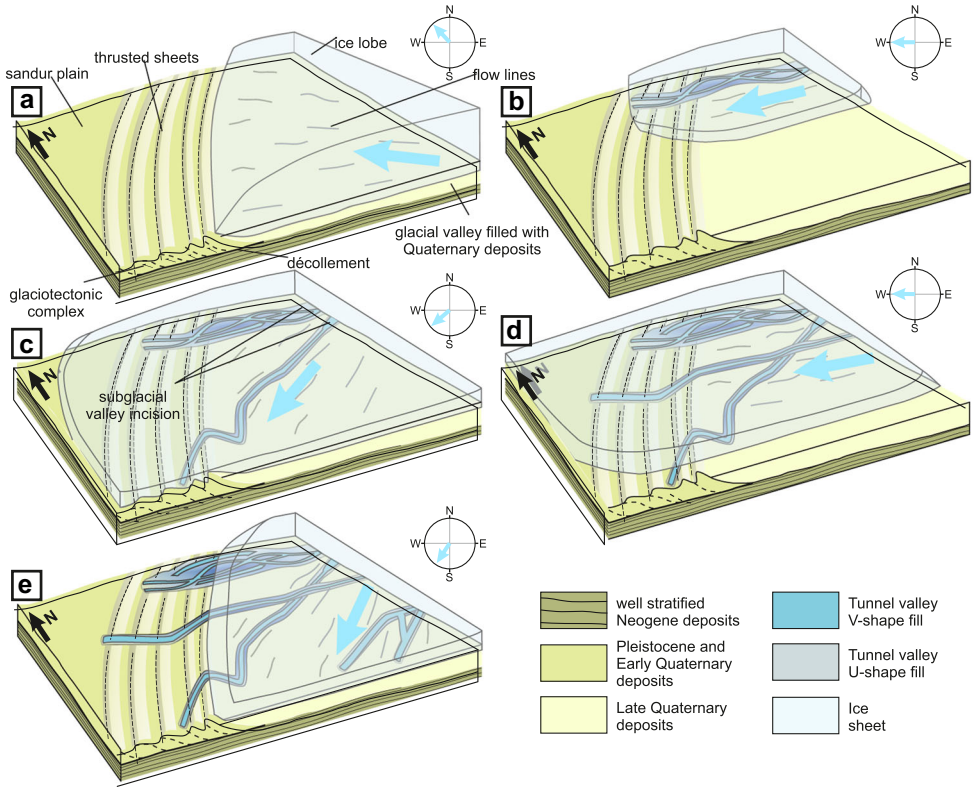

Figure 13. Schematic subplots showing multiple possible ice margins in the study area resulting in glaciotectonic thrust sheets and multiple tunnel valleys with different orientations. Subplots show progressively younger ice margins from (a) to (e). Each subplot is accompanied with a sense of forward direction of the ice margin (top right). The relative chronology is inferred from cross-cutting relationships in the seismic data. [Color figure can be viewed at wileyonlinelibrary.com]

Conclusions

This study imaged tunnel valleys in the German sector of the southeastern North Sea in very high detail. These data shed light on the complex formation of tunnel valleys and an associated GTC. Based on our results and previous research in the area, we assume that the deep tunnel valleys in the study area (TV1–TV3) are older (formed during the Elsterian glaciation), whereas the shallower tunnel valleys (TV4–TV5) are younger (possibly formed during the Saalian complex). However, in the absence of age control, we are unable to assign definitive absolute ages to the structures apart from their relative time of formation.

We conclude that pressurised subglacial meltwater was responsible for their formation. The complex fill and incision directions indicate that a number of ice advances covered the study area. The direction of incision as well as the direction of thrusting in the GTC advocate for different orientations of several ice advances during a previous glaciation of the North Sea. An arcuate shape of the ice margin is likely the reason for the thrust directions transitioning from north to west.

The study shows that the classic model of few continental-scale advances during former glaciations does not hold true. Rather it seems that ice sheets have been highly dynamic and their margin changed shape and direction over short time scales, resulting in complex incision patterns of buried tunnel valleys and glaciotectonic deformation.

Supporting information

Additional supporting information may be found in the online version of this article at the publisher's web-site.

Figure S1. Compilation of seismic sections imaging tunnel valley 1 (TV1) from east to west on multiple parallel lines. TV1 is kept in the middle of the plot. Inset gives location of the seismic section.

Figure S2. Compilation of seismic sections imaging tunnel valley 2 (TV2) from east to west on multiple parallel lines. TV2 is kept in the middle of the plot. Inset gives location of the seismic section.

Figure S3. Compilation of seismic sections imaging tunnel valley 3 (TV3) from east to west on multiple parallel lines. TV3 is kept in the middle of the plot. Inset gives location of the seismic section.

Acknowledgements. We would like to thank the State Agency for Coastal Protection, National Park and Nature Protection of Schleswig-Holstein and the State Agency for Agriculture, Environment and Rural Areas of Schleswig-Holstein for funding this work as part of the project 'Nordfriesland Süd – the geological/sedimentological architecture and habitat distribution in the transition area Wadden Sea – Shelf between the Amrum Bank and the Eider Channel (North Sea)'.

Additionally we would like to thank the crew of *R/V ALKOR* during expedition AL496 and the technicians as well as the students helping in the data acquisition.

Our gratitude goes to Stephen Livingstone and an anonymous reviewer, whose insightful reviews have substantially improved the manuscript. Open access funding enabled and organized by Projekt DEAL.

Data availability statement

The data that support the findings of this study are available from the corresponding author upon reasonable request. The data are not publicly available due to legal restrictions.

Authorship

AL has written the article and processed the data used for the article. SK, KS, DU and AO gave valuable input for the

streamlining of the article and provided additional information on the study area. SK and KS led the data acquisition, which was aided by AL and DU. All authors have contributed with valuable comments, discussions and guidance for the improvement of the article.

Conflicts of interest—The authors declare no conflicts of interest.

References

Aber JS, Ber A. 2007. *Glaciotectonism* 6th ed. Elsevier: Amsterdam.

Al Hseinat M, Hübscher C. 2014. Ice-load induced tectonics controlled tunnel valley evolution - instances from the southwestern Baltic Sea. *Quaternary Science Reviews* **97**: 121–135.

Batchelor CL, Margold M, Krapp M *et al*. 2019. The configuration of Northern Hemisphere ice sheets through the Quaternary. Nature *Communications* **10**: 1–10.

Benediktsson ÍÖ, Schomacker A, Johnson *et al*. 2015. Architecture and structural evolution of an early Little Ice Age terminal moraine at the surge-type glacier Múlajökull, Iceland. *Journal of Geophysical Research–Earth Surface* **120**: 1895–1910.

Boulton GS, Hindmarsh RCA. 1987. Sediment deformation beneath glaciers: rheology and geological consequences. *Journal of Geophysical Research* **92**: 9059–9082.

BURVAL Working Group. 2009. Buried Quaternary valleys – a geophysical approach. Zeitschrift der Dtsch. *Gesellschaft fur Geowissenschaften* **160**: 237–247.

Clayton L, Attig JW, Mickelson DM. 1999. Tunnel channels formed in Wisconsin during the last glaciation. *Special Papers – Geological Society of America* **337**: 69–82.

Cotterill C, Phillips E, James L *et al*. 2017. How understanding past landscapes might inform present-day site investigations: A case study from Dogger Bank, southern central North Sea. *Near Surface Geophysics* **15**: 403–413.

Coughlan M, Fleischer M, Wheeler *et al*. 2018. A revised stratigraphical framework for the Quaternary deposits of the German North Sea sector: a geological-geotechnical approach. *Boreas* **47**: 80–105.

Dove D, Evans DJA, Lee JR *et al*. 2017. Phased occupation and retreat of the last British–Irish Ice Sheet in the southern North Sea; geomorphic and seismostratigraphic evidence of a dynamic ice lobe. *Quaternary Science Reviews* **163**: 114–134.

Dowdeswell JA, Canals M, Jakobsson M *et al*. 2016. The variety and distribution of submarine glacial landforms and implications for ice-sheet reconstruction. *Geological Society, London, Memoirs* **46**: 519–552.

Ehlers J. 1990. Reconstructing the Dynamics of the North-West European Pleistocene Ice Sheets. *Quaternary Science Reviews* **9**: 71–83.

Ehlers J, & Gibbard PL. 2004. Quaternary glaciations-extent and chronology: part I. Europe J. Ehlers & Philip L. Gibbard (eds). Amsterdam, The Netherlands: Elsevier.

Ehlers J, Gibbard PL, Hughes PD. 2018. *Quaternary Glaciations and Chronology, Past Glacial Environments*. Second Edition. Elsevier: Amsterdam.

Ehlers J, Grube A, Stephan H-J *et al*. 2011. Pleistocene glaciations of North Germany-New results. *Developments in Quaternary Sciences* **15**: 149–162.

Ehlers J, Linke G. 1989. The origin of deep buried channels of Elsterian age in Northwest Germany. *Journal of Quaternary Science* **4**: 255–265.

Ehlers J, Mayer K-D, Stephan H-J. 1984. The pre-weichselian glaciations of north-west europe. *Quaternary Science Reviews* **3**: 1–40.

GeoSeaPortal. 2019. Bathymetric data set of the Federal Maritime and Hydrographic Agency of Germany. Online: https://www.geoseaportal.de/mapapps/ (Accessed 15 August 2019).

Ghienne JF, Deynoux M. 1998. Large-scale channel fill structures in Late Ordovician glacial deposits in Mauritania, western Sahara. *Sedimentary Geology* **119**: 141–159.

Gibling MR. 2006. Width and Thickness of Fluvial Channel Bodies and Valley Fills in the Geological Record: A Literature Compilation and Classification. *International Journal of Sediment Research* **76**: 731–770.

Greenwood SL, Clason CC, Helanow C *et al*. 2016. Theoretical, contemporary observational and palaeo-perspectives on ice sheet hydrology: Processes and products. *Earth-Science Reviews* **155**: 1–27.

Hinsch W. 1979. Rinnen an der Basis des glaziaren Pleistozäns in Schleswig-Holstein. *Eiszeitalter und Gegenwart* **29**: 173–178.

Huuse M. 2002. Late Cenozoic palaeogeography of the eastern North Sea Basin: Climatic vs tectonic forcing of basin margin uplift and deltaic progradation. *Bulletin of the Geological Society of Denmark* **49**: 145–170.

Huuse M, Le Heron DP, Dixon R *et al*. 2012. Glaciogenic reservoirs and hydrocarbon systems: An introduction. *Geological Society Special Publication* **368**: 1–28.

Huuse M, Lykke-Andersen H. 2000. Overdeepened Quaternary valleys in the eastern Danish North Sea: Morphology and origin. *Quaternary Science Reviews* **19**: 1233–1253.

Jansen JD, Codilean AT, Stroeven AP *et al*. 2014. Inner gorges cut by subglacial meltwater during Fennoscandian ice sheet decay. *Nature Communications* **5**: 1–7.

Jørgensen F, Sandersen PBE. 2006. Buried and open tunnel valleys in Denmark-erosion beneath multiple ice sheets. *Quaternary Science Reviews* **25**: 1339–1363.

Kehew AE, Piotrowski JA, Jørgensen F. 2012. Tunnel valleys: Concepts and controversies - A review. *Earth-Science Reviews* **113**: 33–58.

Kluiving SJ, Aleid Bosch JH, Ebbing *et al*. 2003. Onshore and offshore seismic and lithostratigraphic analysis of a deeply incised Quaternary buried valley system in the Northern Netherlands. *Journal of Applied Geophysics* **53**: 249–271.

Kockel F. 2002. Rifting processes in NW-Germany and the German North Sea sector. *Netherlands Journal of Geosciences* **81**: 149–158.

Kristensen TB, Huuse M, Piotrowski J *et al*. 2007. A morphometric analysis of tunnel valleys in the eastern North Sea based on 3D seismic data. *Journal of Quaternary Science* **22**: 801–815.

Kristensen TB, Piotrowski JA, Huuse M *et al*. 2008. Time-transgressive tunnel valley formation indicated by infill sediment structure, North Sea – the role of glaciohydraulic supercooling. *Earth Surface Processes and Landforms* **33**: 546–559.

Lambeck K, Purcell A, Funder S *et al*. 2006. Constraints on the Late Saalian to early Middle Weichselian ice sheet of Eurasia from field data and rebound modelling. *Boreas* **35**: 539–575.

Lang J, Winsemann J, Steinmetz D *et al*. 2012. The Pleistocene of Schöningen, Germany: A complex tunnel valley fill revealed from 3D subsurface modelling and shear wave seismics. *Quaternary Science Reviews* **39**: 86–105.

Le Heron D, Sutcliffe O, Bourgig K *et al*. 2004. Sedimentary architecture of Upper Ordovician tunnel valleys, Gargaf Arch, Libya: Implications for the genesis of a hydrocarbon reservoir. *GeoArabia* **9**: 137–160.

Lewis AR, Marchant DR, Kowalewski DE *et al*. 2006. The age and origin of the Labyrinth, western Dry Valleys, Antarctica: Evidence for extensive middle Miocene subglacial floods and freshwater discharge to the Southern Ocean. *Geology* **34**: 513–516.

Livingstone SJ, Clark CD. 2016. Morphological properties of tunnel valleys of the southern sector of the Laurentide Ice Sheet and implications for their formation. *Earth Surface Dynamics* **4**: 567–589.

Lokhorst A, Adlam K, Brugge JVM *et al*. 1998. NW European Gas Atlas--composition and isotope ratios of natural gases. GIS application on CD-ROM by the British Geological Survey, Bundesanstalt für Geowissenschaften und Rohstoffe, Danmarks og Gronlands Geologiske, Undersogelse, Netherlands Instituut voor Toegepaste geowetenschappen, Panstwowy Instytut Geologiczny, European Union.

Lonergan L, Maidment SCR, Collier JS. 2006. Pleistocene subglacial tunnel valleys in the central North Sea basin: 3-D morphology and evolution. *Journal of Quaternary Science* **21**: 891–903.

Lutz R, Kalka S, Gaedicke C *et al*. 2009. Pleistocene tunnel valleys in the German North Sea: spatial distribution and morphology. *Zeitschrift der Dtsch. Gesellschaft für Geowissenschaften* **160**: 225–235.

Moores HD. 1989. On the Formation of the Tunnel Valleys of the Superior Lobe, Central Minnesota. *Quaternary Research* **32**: 24–35.

Moreau J, Huuse M, Janszen A *et al*. 2012. The glaciogenic unconformity of the southern North Sea. *Geological Society Special Publication* **368**: 99–110.

Mullins HT, Hinchey EJ. 1989. Erosion and infill of New York Finger Lakes: Implications for Laurentide ice sheet deglaciation. *Geology* **17**: 622–625.

Ó Cofaigh C. 1996. Tunnel Valley Genesis. *Encyclopedia of Environmental Change* **20**: 1–19.

Ottesen D, Stewart M, Brönner M *et al*. 2020. Tunnel valleys of the central and northern North Sea (56°N to 62°N): Distribution and characteristics. *Marine Geology* **425**: 106199.

Overeem I, Weltje GJ, Bishop-Kay C *et al*. 2001. The Late Cenozoic Eridanos delta system in the Southern North Sea Basin: A climate signal in sediment supply? *Basin Research* **13**: 293–312.

Patterson CJ. 1994. Tunnel-valley fans of the St. Croix moraine, east-central Minnesota, USA. In Meeting of the commision on the formation and deformation of glacial deposits (1991-05): 69–87.

Piotrowski JA. 2007. Groundwater Under Ice Sheets and Glaciers. In *Glacier Science and Environmental Change*, Knight PG (ed.). Blackwell Science: Oxford; 50–60.

Piotrowski JA. 1994. Tunnel-valley formation in northwest Germany-geology, mechanisms of formation and subglacial bed conditions for the Bornhöved tunnel valley. *Sedimentary Geology* **89**: 107–141.

Praeg D. 2003. Seismic imaging of mid-Pleistocene tunnel-valleys in the North Sea Basin-high resolution from low frequencies. *Journal of Applied Geophysics* **53**: 273–298.

Praeg D. 1996. Morphology, stratigraphy and genesis of buried Mid-Pleistocene tunnel-valleys in the Southern North Sea Basin. University of Edinburgh: United Kingdom.

Praeg D, Long D. 1997. Buried Sub- and Proglacial Channels: 3D-Seismic Morphostratigraphy. In *Glaciated Continental Margins: An Atlas of Acoustic Images*, Davies TA, Bell T, Cooper AK *et al*. (eds.), Springer Netherlands: Dordrecht; 66–67.

Prins LT, Andresen KJ. 2019. Buried late Quaternary channel systems in the Danish North Sea – Genesis and geological evolution. *Quaternary Science Reviews* **223**: 105943.

Sandersen PBE, Jørgensen F. 2003. Buried Quaternary valleys in western Denmark-occurrence and inferred implications for groundwater resources and vulnerability. *Journal of Applied Geophysics* **53**: 229–248.

Sandersen PBE, Jørgensen F, Larsen NK *et al*. 2009. Rapid tunnel-valley formation beneath the receding Late Weichselian ice sheet in Vendsyssel, Denmark. *Boreas* **38**: 834–851.

Sejrup HP, Aarseth I, Haflidason H. 1991. The Quaternary succession in the northern North Sea. *Marine Geology* **101**: 103–111.

Stackebrandt W. 2009. Subglacial channels of Northern Germany–a brief review. *Zeitschrift der Dtsch. Gesellschaft für Geowissenschaften* **160**: 203–210.

Stewart MA, Lonergan L. 2011. Seven glacial cycles in the middle-late Pleistocene of northwest Europe: Geomorphic evidence from buried tunnel valleys. *Geology* **39**: 283–286.

Stewart MA, Lonergan L, Hampson G. 2013. 3D seismic analysis of buried tunnel valleys in the central North Sea: Morphology, cross-cutting generations and glacial history. *Quaternary Science Reviews* **72**: 1–17.

Thöle H, Gaedicke C, Kuhlmann G *et al*. 2014. Late Cenozoic sedimentary evolution of the German North Sea—A seismic stratigraphic approach. *Newsletters on Stratigraphy* **47**: 299–329.

Ussing NV, Selskab DKDV. 1903. Om jyllands Hedesletter og Teorierne for deres Dannelse, Oversigt over Det Kongelige Danske Videnskabernes Selskabs Forhandlinger.

Van der Vegt P, Janszen A, Moscariello A *et al*. 2012. Tunnel valleys: current knowledge and future perspectives, *Geological Society of London Special Publications* 368: 75 LP–97.

Winsemann J, Koopmann H, Tanner DC *et al*. 2020. Seismic interpretation and structural restoration of the Heligoland glacio-tectonic thrust-fault complex: Implications for multiple deformation during (pre-)Elsterian to Warthian ice advances into the southern North Sea Basin. *Quaternary Science Reviews* **227**: 1–15.

Woldstedt P. 1922. Studien an Rinnen und Sanderflächen in Norddeutschland. *Zeitschrift der Dtsch. Geol. Gesellschaft* **74**: 130–133.

Woodland AW, Woodland BYAW. 1970. The Buried Tunnel-Valleys of East Anglia. *Proceedings of the Yorkshire Geological Society* **37**: 521 LP–578.

Wright HE. 1973. Tunnel valleys, glacial surges, and subglacial hydrology of the Superior Lobe, Minnesota. *Geological Society of America Memoirs* **136**: 251–276.

Ziegler PA. 1990. Geological atlas of western and central Europe. Geological Society of London.

